Quantification of Mixing and Mixing Rate from Experimental Observations

R. Everson,* D. Manin,† L. Sirovich‡

The Rockefeller University, New York, NY.

M. Winter§

United Technologies Research Center, East Hartford, CT.

Abstract

Experimental datasets from a variety of mixing flows are analyzed to assess the degree of mixing and the rate of mixing. The concentration field of an axisymmetric jet is measured at ten downstream locations by optical imaging of Rayleigh scattering from a laser sheet. A new measure of *mixedness*, based on entropy considerations, and a related *mixing rate* is calculated for each of the locations. In agreement with theory, *the mixedness of the self-similar jet is constant along the length of the jet.* The measures allow us to locate the instantaneous realization that is the most typical in terms of mixedness and mixing rate.

Also analyzed is the mixing of a row jets injecting fluid into a crossflow. The jets are sufficiently close that there is significant interaction between neighboring jets. The mixedness and mixing rate were calculated. Well mixed regions have a low mixing rate, while poorly mixed regions tend to mix most rapidly. The mixedness and mixing rate allow the assessment of the effectiveness of different orifice shapes in promoting rapid mixing.

Introduction

Mixing processes play a vital role in the operation of combustors for air-breathing propulsion systems. This paper is primarily concerned with the nature of these mixing processes and how they may be assessed in quantitative terms from data acquired using advanced laser imaging techniques. A longer range goal of this research is to develop methods and criteria for the management and prediction of the mixing process. Although the principal focus is a specific gas turbine combustor problem, the methodology developed is equally applicable to virtually every aspect of technology and engineering where mixing processes are important.

An example of a mixing-dominated problem is the gas turbine combustor. The design and performance of a gas turbine combustor requires good mixing characteristics to achieve high burning rates, low soot and oxides of nitrogen (NO_x) formation, and exhaust temperature uniformity. Typically, however, complete mixing can only be accomplished at the expense of combustor length and pressure loss. A gas turbine combustor flow path is characterized by three distinct zones: a primary zone, where combustion occurs; an intermediate zone, where mixing-driven species recombination (to lower gas temperatures) occurs; and a dilution zone, where coolant air is injected and mixed with the combustion gases to achieve a desired turbine inlet temperature. Specific geometries[1] for the High-Speed Civil Transport (HSCT), rely on either fast mixing before injection to the combustor, or in a quench zone downstream of a rich combustion zone, to achieve low NO_x emissions. Current designs for these dilution or quench zones resort to a series of round jets, or other geometric shapes, injecting cold air at right angles to the primary gas flow to achieve the highest degree of mixing. The Rich-burn/Quick-mix/Lean-burn (RQL) combustor uses axially staged burning zones to avoid stoichiometric mixtures in order to minimize NO_x production, while maintaining a high level of combustor efficiency. The quick-mix section is a key technology for this combustor to achieve low emission. The rate of mixing, however, is strongly influenced by the hole shape, mo-

---

*Assistant Professor, Rockefeller University.

†Post-doctoral Research Associate, Rockefeller University.

‡Visiting Professor, Rockefeller University.

§Manager, Advanced Optical Diagnostics, Member AIAA.

mentum ratio of the jet/primary flow, turbulence level, axial distance, etc.

To date, mixing optimization has been largely an empirical process, and any assessment of induced mixing has been indirectly inferred. Efficient design of such machines requires quantitative information about the degree and rate of mixing attained for different configurations. Laser diagnostic techniques, including Lorentz/Mie,[2] Rayleigh[3] and Raman[4] scattering, and planar laser induced fluorescence[5–8] allow quantitative measurements of the concentration field at single instants in time. While these techniques continue to mature and begin to be used in the design of combustion systems, adequate means of ascertaining quantitative measures of mixing from these data still needs to be addressed.

Perhaps the coarsest and most widespread measure of a passive scalar field is the root mean square value of fluctuations of concentration about the mean:

$$\langle(\rho(\mathbf{x}) - \langle\rho(\mathbf{x})\rangle)^2\rangle^{1/2} , \tag{1}$$

where $\rho(\mathbf{x})$ denotes the concentration of the passive scalar at $\mathbf{x}$ and angle brackets denote the ensemble average. The smaller the average RMS fluctuation the better mixed is the flow. However, although (1) furnishes us with information that locates and measures the fluctuations, it does not address the scales of the fluctuations or the rate at which mixing occurs. Dahm and Dimotakis[9] have examined mixing and entrainment in turbulent jets, paying particular attention to the large scale, organized motions. Winter *et. al.*[10] have examined other mixing measures.

The present study will focus on a model problem of the dilution or quench zone, viz., a subsonic jet in a crossflow. Such problems have been previously studied experimentally by Vranos and Liscinsky.[11] In their experiment, advanced data acquisition techniques using optically based diagnostics[12] furnish us with a wealth of detailed and highly resolved data. Although the data that will be analyzed are from a physical experiment, the methodology presented is applicable generally and could just as easily have been applied to a computationally generated data base.

In this paper we advance new measures of mixedness and mixing rate, and apply them to experiments. The first experiment examines the relatively simple axisymmetric jet. The second models the quench zone of a gas turbine combustor and consists of a pair of directly opposed rows of jets injecting fluid into a crossflow. In the following section we describe the experimental arrangements. The measures of mixing and mixing rate are then introduced, after which we discuss the results of applying them to the experimental data.

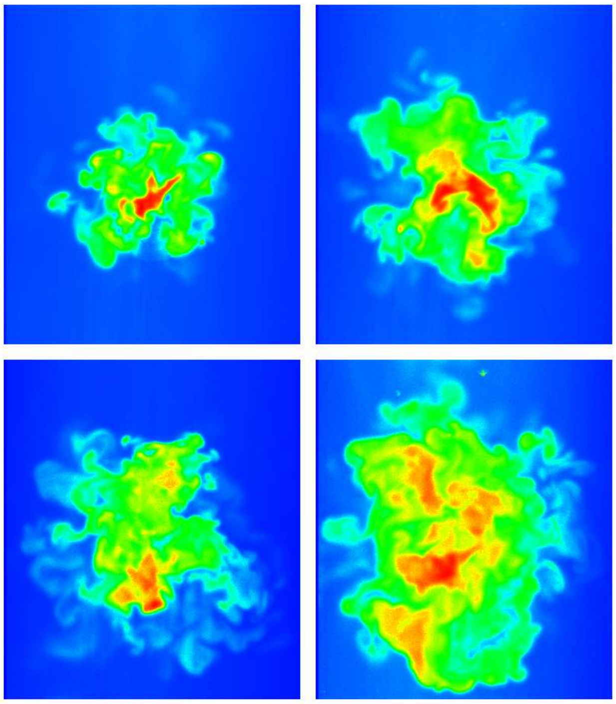

Figure 1: Typical snapshots of the concentration field from an axisymmetric jet at 2, 4, 6 and 8 jet diameters downstream from the orifice.

Description of Experiments

Axisymmetric jet

In the first experiment, an axisymmetric jet, equipped with a co-flow, was used to flow propane through a central orifice of diameter 4 mm. The Reynolds number based on the orifice diameter was 8000. The flow was intersected at $1, 2, ..., 10$ diameters downstream by a sheet of 532nm laser light produced by a Nd:YAG laser. The Rayleigh scattered light was recorded on an unintensified, thermo-electrically cooled CCD camera. The purpose of the coflow (velocity 5cm/s) was to prevent extraneous dust from entering the imaged region. After correction for background and optical response, images were obtained in which the intensity was proportional to the flow field concentration. Typical images from 2, 4, 6 and 8 diameters downstream are shown in Figure 1. We remark that instantaneous profiles are "top hat" shaped, rather than decaying smoothly like the mean profile (not shown). This observation is in agreement

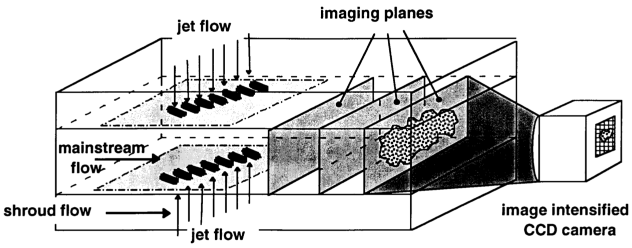

Figure 2: Schematic diagram of the RQL model experiment.

with that of Dahm & Dimotakis:[9] it implies that unmixed fluid is entrained deep into the jet and suggests that the jet is poorly characterized by the mean profile.

RQL model

The second experiment was directed toward jets in confined crossflow. The data acquisition system is described in detail in.[12] Figure 2 is a schematic representation of the apparatus, which consisted of three parallel contiguous ducts of rectangular cross section, simulating a sector of an annular combustor. Sector width was 305mm and the inner duct height was set at 50.8mm for the reported experiments. The outer ducts (shrouds), which supply the injectant gas, were 25mm in height. These are separated from the inner duct by removable, 3mm thick flat plates. The injectant was fed from the shrouds to the inner duct through orifices of various sizes and shapes machined into the plates. Jet fluid was injected from the upper and lower walls through orifices consisting of either round holes or slanted slots (see Figure 2). Mass flow to each of the three ducts was controlled independently using venturi flowmeters. The maximum variation in the mean approach velocity of the mainstream flow was 6% with a turbulence level of 1.3%. Air was both the injectant and central duct fluid, so that the density ratio was one.

Planar digital imaging was used to optically measure concentration distributions in planes perpendicular to the duct axis, starting at the leading-edge of the orifice and continuing downstream to a location equal to the duct height. The Mie scattering technique[5] was used by marking the jet flow with an oil aerosol of sub-micron sized particles. A light sheet (0.5mm thick) was created using a 2W argon-ion laser and a rotating mirror. The flow field was illuminated by passing the light sheet through a window in the side wall of the test section. An image intensified thermo-electrically cooled CCD camera (Photometrics Star 1), located inside the duct 0.76m downstream of the orifice centerline, was focused on the illuminated plane to provide an end-on view. The camera was synchronized to make instantaneous exposures coincident with the sweep of the beam through the flow field. The image was digitized and sent to a computer for storage. (The data acquisition scheme is described in detail in.[12]) After correction for background and response, the scattered light intensity was proportional to the number of particles in the measurement volume. If only one of two streams is marked (in this study the jet fluid), the light intensity of the undiluted marked fluid

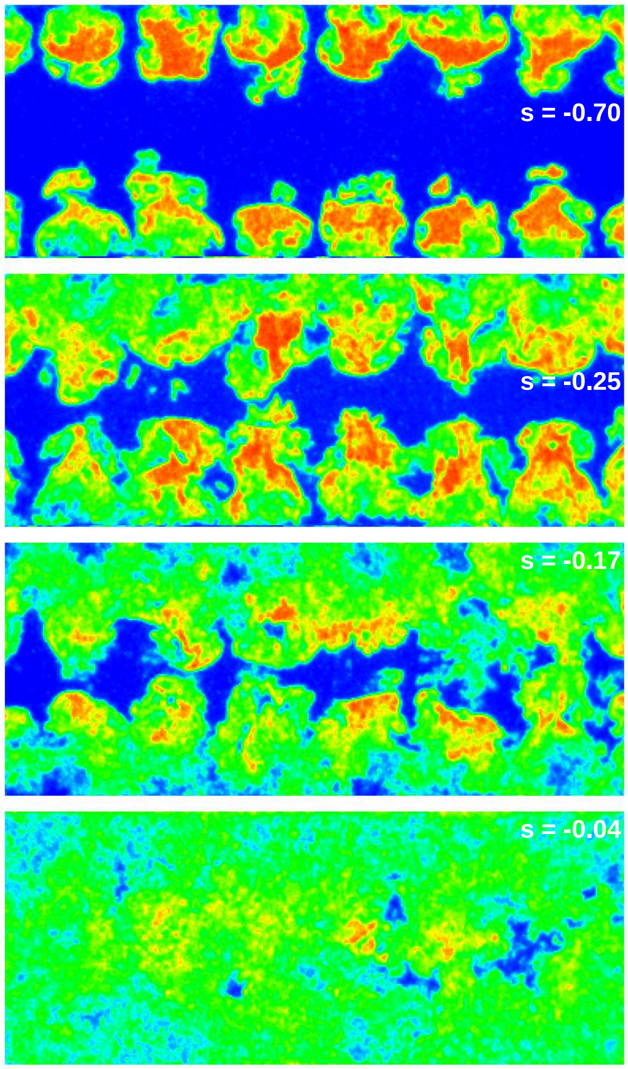

Figure 3: Typical snapshots of the concentration field downstream from two opposing rows of circular injectors. Fluid is injected vertically from the top and bottom of the pictures and the crossflow is directed out of the picture. The snapshots are at 0.87, 1.28, 1.88 and 4.26 diameters downstream of the center of the orifices. Each snapshot is labeled with its entropy, s, which measures its mixedness, as discussed in the text.

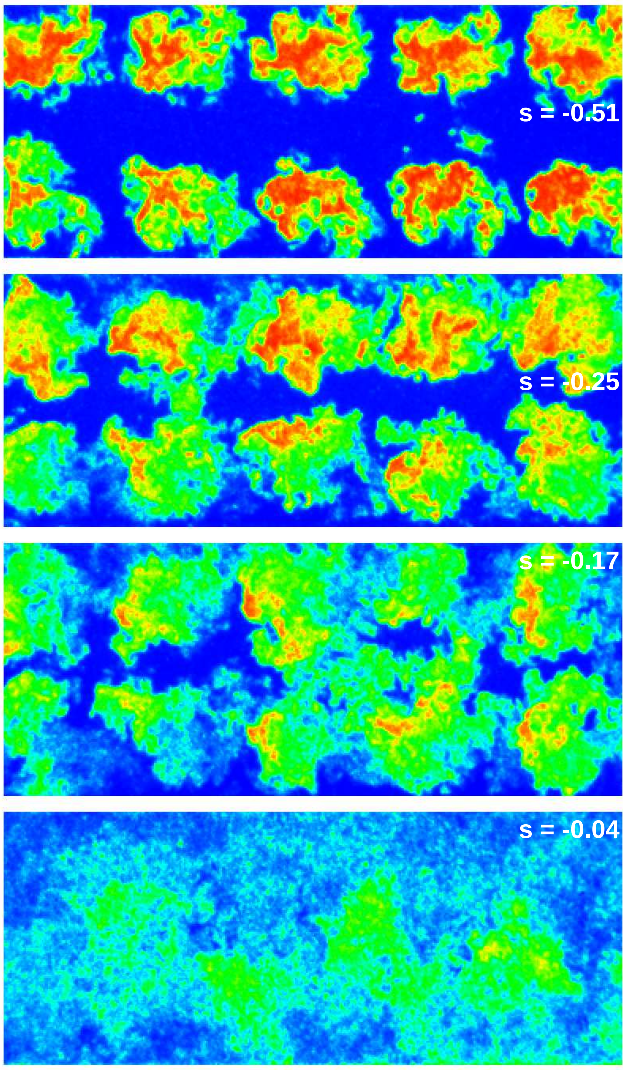

Figure 4: Typical snapshots of the concentration field downstream from two opposing rows of slanted slot injectors. Measured in units of the diameter of a circular orifice with the same diameter, the snapshots are at 0.63, 1.0, 1.64 and 4.00 diameters downstream of the center of the orifices.

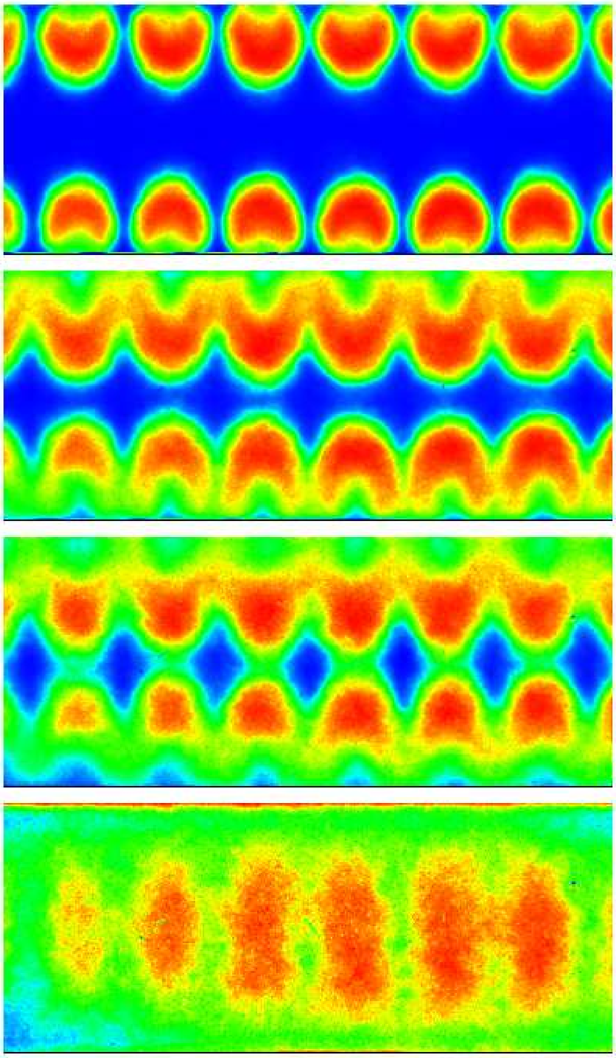

Figure 5: Average concentration field downstream from two opposing rows of circular injectors.

represents mole fraction unity. Instantaneous realizations of the mole fractions at four different downstream locations are shown in Figures 3 and 4 for round holes and slanted slots respectively. In the figures fluid is injected vertically from orifices at the top and bottom edges of the picture into a crossflow out of the page. One hundred realizations each recorded in a 576×388 format, with 10 bit resolution, were recorded at each downstream location for each of the two injectors. Average concentration fields are shown in Figures 5 & 6. Here too, the smoothly decaying average concentrations are poor representatives of the instantaneous concentration profiles produced as unmixed ambient fluid is entrained close to the cores of the jets.

Mixedness and mixing rate

In this section we introduce a new measure of mixedness, based on entropy and relate it to the rate of mixing in the fluid. The basic approach follows arguments given in statistical mechanics.[13] We mention in passing that Pope[14] has used an entropy principle to obtain probability distribution functions in related flows. We proceed generally and partition the concentration field, $\rho(\mathbf{x})$, into a grid of cells. For the present ρ represents the concentration in three dimensions. If the mixing species is comprised of n identical molecules we denote

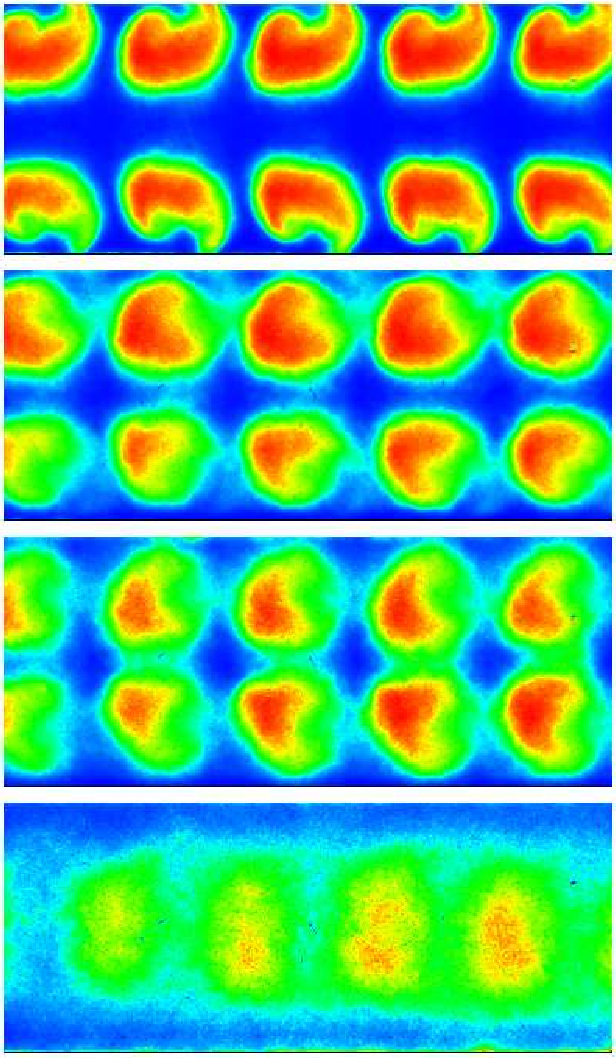

Figure 6: Average concentration field downstream from two opposing rows of slanted slot injectors.

the number of molecules in the l^{th} cell as n_l, so that if the cell centered at has volume $\delta\mathbf{x}$, $\mathbf{x}_l$

$$\rho(\mathbf{x}_l)\delta\mathbf{x} \;\approx\; n_l \tag{2}$$

and

$$\sum_l n_l \;=\; n \;. \tag{3}$$

The measured concentration distribution can be achieved by

$$\frac{n!}{n_1!n_2!...n_l!} \tag{4}$$

arrangements of the molecules (not counting those arrangements which are indistinguishable). When the fluid is poorly mixed so that the molecules are concentrated in just a few cells the number of distinct arrangements is small compared with a uniformly mixed fluid in which there are the same number of molecules in each cell. The configurational entropy of the distribution is

$$S \;=\; \ln\frac{n!}{\prod_l n_l!} \;=\; \ln n! - \sum_l \ln n_l! \tag{5}$$

If we use Stirling's approximation, i.e., $\ln m! \approx m\ln m - m$ we obtain

$$S \;\approx\; n\ln n - \sum_l \ln n_l \;. \tag{6}$$

Since entropy is indeterminate up to a constant we can drop $n\ln n$ and write:

$$S \;=\; -\sum_l n_l \ln n_l \;. \tag{7}$$

Since $n_l = \rho(\mathbf{x}_l)\delta\mathbf{x}$, where $\delta\mathbf{x}$ is the volume element, we have

$$S \;=\; -\sum_l \rho(\mathbf{x}_l)\delta\mathbf{x}(\ln\rho(\mathbf{x}_l) + \ln\delta\mathbf{x}) \tag{8}$$

and as $\delta\mathbf{x} \to 0$

$$S \;=\; -\int \rho\ln\rho \; d\mathbf{x} \;-\; \ln\delta\mathbf{x}\int\rho \; d\mathbf{x} \;. \tag{9}$$

The second term is a constant and therefore, modulo a constant, the entropy is measured by

$$S \;=\; -\int \rho(\mathbf{x})\ln\rho(\mathbf{x}) \;\; d\mathbf{x} \;. \tag{10}$$

Next, we consider we deal with entropy per density, $s = S/\rho_0$, where ρ_0, is a reference value. Then, up to a constant, s is given by

$$s \;=\; -\int \frac{\rho}{\rho_0}\ln\frac{\rho}{\rho_0}\; d\mathbf{x} \;=\; -\int \sigma\ln\sigma \; d\mathbf{x} \tag{11}$$

Figure 7 exhibits the entropy for four different snapshots. These data are Mie scattering images collected downstream of two rows of round holes injecting fluid. The entropy clearly agrees with the intuitive notion of mixedness: the panels with high entropy are better mixed than those with low entropy. It should be remarked that all four panels come from a single flow condition. The wide variation in mixedness make visual assessment of the average degree of mixing difficult. The average entropy, however, characterizes the mean mixedness.

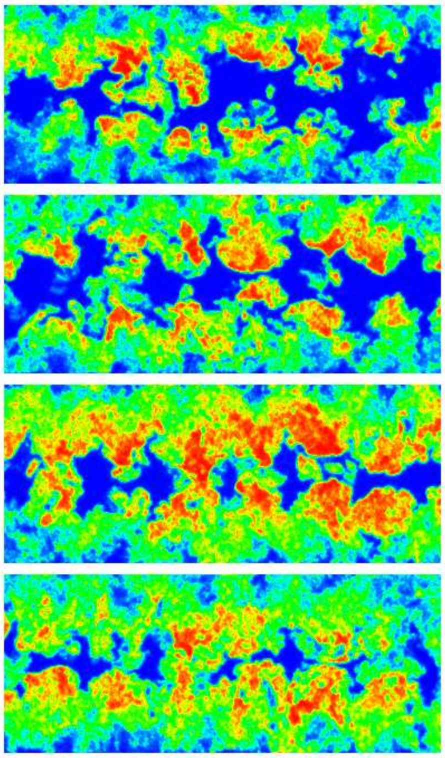

Figure 7: Entropy as a measure of mixedness. The four snapshots, all from the same station under the same flow conditions, are marked with the entropy s that measures the mixedness of the snapshot.

Also shown is the RMS concentration fluctuation $[\int(\rho - \rho_0)^2 d\mathbf{x}]^{1/2}$, for each frame. The entropy distinguishes between the middle frames, which have the same RMS fluctuation. We point out that when the fluctuations are small, so that $\rho(\mathbf{x}) \approx \rho_0(1 + \epsilon\rho'(\mathbf{x}))$ and $\int \rho(\mathbf{x}) d\mathbf{x} = 0$, the entropy is well approximated by the RMS fluctuation divided by the mean concentation.

Although we wish to apply our deliberations to snapshots, hence two-dimensional fields, it is advantageous to continue to develop the framework in three dimensions. We start with the diffusion equation,

$$\frac{\partial \sigma}{\partial t} + \nabla.(\sigma \mathbf{u}) \;=\; \kappa \nabla^2 \sigma \;, \tag{12}$$

which governs mixing. The (turbulent) flow $\mathbf{u}$ is taken to be incompressible, $\nabla.\mathbf{u} = 0$. Data analysis of concentration fields is based on averages over many images, and thus among other reasons, we should consider ensemble averages. This will be denoted by brackets or bars, e.g.,

$$\langle \mathbf{u} \rangle \;=\; \bar{\mathbf{u}} \;. \tag{13}$$

If we write

$$\mathbf{u} \;=\; \bar{\mathbf{u}} + \mathbf{u}' \;, \tag{14}$$

then it follows that

$$\nabla.\bar{\mathbf{u}} \;=\; 0 \;=\; \nabla.\mathbf{u}' \;. \tag{15}$$

If (14) is substituted into (12) and an ensemble average performed, we obtain

$$\frac{\partial \bar{\sigma}}{\partial t} + \nabla.(\bar{\sigma}\bar{\mathbf{u}}) + \nabla.(\overline{\sigma \mathbf{u}'}) \;=\; \kappa \nabla^2 \bar{\sigma} \;. \tag{16}$$

For conceptual purposes it is convenient to replace the turbulent mixing, $\overline{\sigma \mathbf{u}'}$, by means of an eddy diffusivity, κ_e, hence

$$\overline{\sigma \mathbf{u}'} \;=\; -\kappa_e \nabla \bar{\sigma} \;. \tag{17}$$

Thus (16) becomes

$$\frac{\partial \bar{\sigma}}{\partial t} + \nabla.(\bar{\sigma}\bar{\mathbf{u}}) \;=\; \nabla.\left[(\kappa + \kappa_e)\nabla \bar{\sigma}\right] \;. \tag{18}$$

We introduce

$$h \;=\; -\int \bar{\sigma} \ln \bar{\sigma} \; d\mathbf{x} \tag{19}$$

which, in the present framework is the counterpart of H in Boltzmann's H-theorem.[15] From this it follows that

$$-\frac{dh}{dt} \;=\; -\int (1 + \ln \bar{\sigma}) \frac{\partial \bar{\sigma}}{\partial t} \; d\mathbf{x} \tag{20}$$

$$= \int \nabla.\left[\bar{\mathbf{u}}\bar{\sigma} \ln \bar{\sigma} - (\kappa + \kappa_e)\nabla \bar{\sigma}\right] \; d\mathbf{x} \tag{21}$$

$$- \int (\kappa + \kappa_e) \frac{(\nabla \bar{\sigma})^2}{\bar{\sigma}} \; d\mathbf{x} \;. \tag{22}$$

Since $\bar{\mathbf{u}}.\mathbf{n} = \mathbf{n}.\nabla \bar{\sigma} = 0$ on the boundaries of the domain it follows that

$$\frac{dh}{dt} \;=\; 4 \int (\kappa + \kappa_e)(\nabla \bar{\sigma}^{1/2})^2 \; d\mathbf{x} \;. \tag{23}$$

Since h measures the mixedness, we call the quantity

$$R \;=\; \int (\nabla \bar{\sigma}^{1/2})^2 \; d\mathbf{x} \tag{24}$$

the *rate of mixing*. A similar quantity for measuring mixing was appears in Winter *et. al.*[10]

To relate these considerations to two-dimensional concentration fields, we, for the moment focus on the case our axisymmetric jet. We denote the streamwise variable by z and integrate (20) in the transverse plane

$$-\frac{\partial}{\partial t} h_2(z,t) = -\frac{\partial}{\partial t} \int \bar{\sigma} \ln \bar{\sigma} \;\; d\mathbf{x} d\mathbf{y}$$

$$= \int \left\{ \frac{\partial}{\partial z}(\mathbf{u}_z \bar{\sigma} \ln \bar{\sigma}) + \nabla_2.(\bar{\mathbf{u}}_2 \bar{\sigma} \ln \bar{\sigma}) \right\} \; d\mathbf{x} d\mathbf{y} \tag{25}$$

$$- \int (1 + \ln \bar{\sigma}) \nabla.\left[\kappa + \kappa_e \nabla \bar{\sigma}\right] \; d\mathbf{x} d\mathbf{y}$$

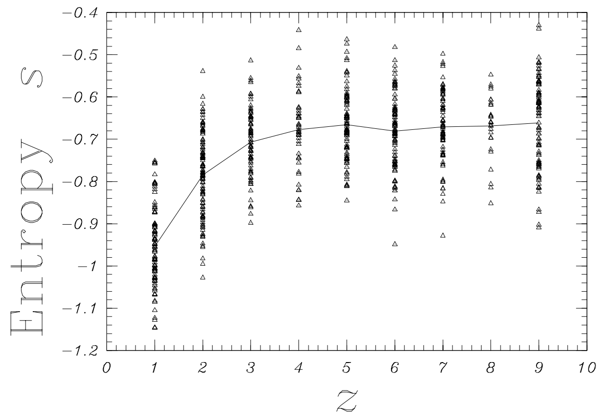

Figure 8: Entropy in the axisymmetric jet as a function of distance from the orifice. Each symbol represents an individual measurement, and the line joins the average entropies at each measurement station. The entropy is calculated over a domain that is normalized to the jet diameter.

Here $\bar{\mathbf{u}}_2 = (\bar{u}_x, \bar{u}_y)$ and $\nabla_2 = (\frac{\partial}{\partial x}, \frac{\partial}{\partial x})$.

In order to proceed further we adopt the reasonable assumption that streamwise derivatives are small compared with transverse derivatives, so that $\nabla.\left[(\kappa+\kappa_e)\nabla\bar{\sigma}\right] \approx \nabla_2\left[(\kappa+\kappa_e)\nabla_2\bar{\sigma}\right]$. On introducing this into the above and proceeding as earlier, we obtain

$$\frac{\partial h_2}{\partial t} + \frac{\partial}{\partial z}(Uh_2) \;=\; 4\int(\kappa+\kappa_e)(\nabla_2\bar{\sigma}^{1/2})^2\,dxdy\;. \tag{26}$$

U is a suitably defined streamwise velocity, e.g., the centerline mean velocity yields a good approximation.

The development just presented furnishes a guide for more general jet flows, viz. we can regard z as the curvilinear distance along the jet centerline and (x, y) as the transverse directions.

Results

Axisymmetric jet

The average entropy, s, and mixing rate, R, were calculated for the axisymmetric jet at $z = 1, 2, ...10$ diameters downstream of the orifice. Unlike the combustor experiment, the jet is not confined to a fixed cross-sectional area, but expands in a self-similar manner so that its radius, $r(z)$, is proportional to the downstream distance, z. (Defining $r(z) = \int \rho r^2 dr / \int \rho r dr$, this was experimentally verified for the jet described here, when $z > 3$ diameters.) Although the jet is not fully self-similar in the region $3 < z < 10$, (i.e., the velocity profiles are not yet self-similar), it is sufficiently far from the orifice for only one length scale, the distance from the orifice, to be relevant. There is no dimensionless combination involving z, other than a constant, on which the entropy (a dimensionless quantity) may depend. Sufficiently far downstream therefore, we may expect the entropy to be constant, provided that an appropriate domain for calculating s is chosen. The correct domain should be consistent with the self-similar expansion of the jet; that is, it should be calculated in a domain that grows in proportion to the jet radius.

Figure 8 shows the average entropy at each of the longitudinal stations, calculated for circular domains embracing the jets, with radii proportional to the local jet radius. The average was taken over $50 - 100$ snapshots. The calculated entropy is consistent with the scaling expected from the self-similar expansion of the jet. The departures at the first two stations may be attributed to the still developing, under-mixed, flow close to the orifice and to residual out-of-focus images of the orifice itself, which are prominent in images recorded at the first station and visible at in those recorded at the second.

RQL Model

The entropy and mixing rate have been calculated for ensembles of concentrations measured downstream of two rows of orifices modeling the injector configuration in a gas turbine combustor. Figure 9 shows the mixing rate, R, plotted against the entropy, s. Each individual symbol corresponds to a particular snapshot, and different symbols denote different locations and orifice shapes (diagonal slots or holes). At locations closest to the orifices the entropy and the mixing rates are high, indicating a poorly mixed flow which is mixing rapidly. Further away from the orifices the flow is better mixed, and the rate of mixing has declined. There is clearly considerable scatter in both the entropy and mixing rate at each location, but the average quantities lie on a well defined locus.

Figure 10 compares the entropy as a function of downstream distance for the mixing flows generated by circular and slanted slot orifices. The area of the slots was equal to the area of the circular holes. Distances are measured from the center of the rows of orifices, and are stated in units of the circular hole diameter. Consequently, the leading and trailing edges of the slots extend further up and downstream than the circular holes. This fact means that the slots begin mixing be-

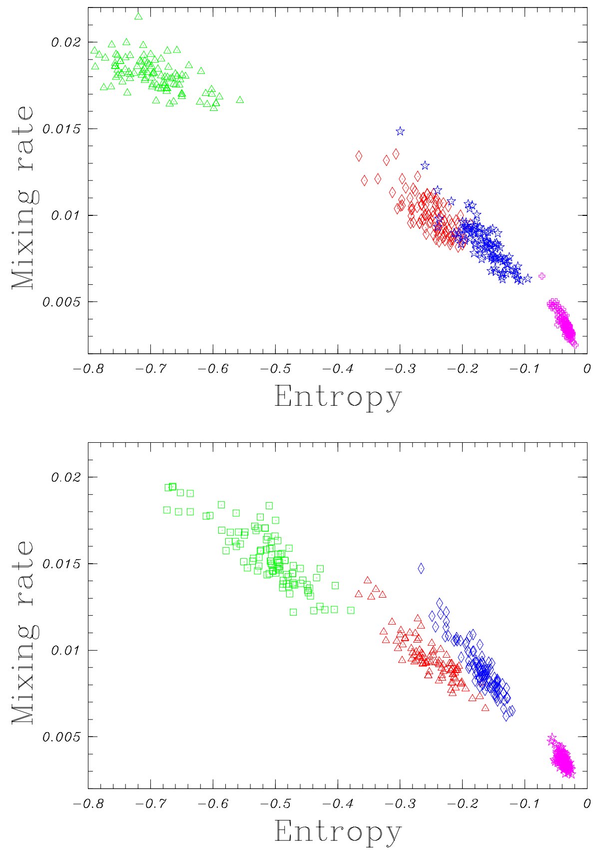

Figure 9: Mixing rate, R, plotted against entropy, s, for (a) circular and (b) slanted slot orifices. Each symbol represents an individual snapshot, and each color a measurement station. For circular holes: green 0.87; red 1.28; blue 1.88; magenta 4.26. For slanted slots: green 0.63; red 1.0; blue 1.64; magenta 4.0.

fore the holes and is reflected by the lower entropy (better mixed) for the slots at less than one diameter downstream. Further downstream, the flows generated by the slots and holes may be said to be equally mixed, and little advantage is to be gained by using one or the other orifice shape. It is to be expected, however, that different orifice shapes will enhance or deplete the rate of mixing in flows where the momentum of the injected fluid is less.

We pause to note the important difference between s, (11), and h, (19). Without averaging we obtain an almost reversible process, in which the relatively small molecular diffusion, κ, accounts for irreversibility. s is the appropriate entropy in this case. With the introduction of averaging the eddy diffusivity, κ_e, appears and h is then the appropriate entropy. Both values of

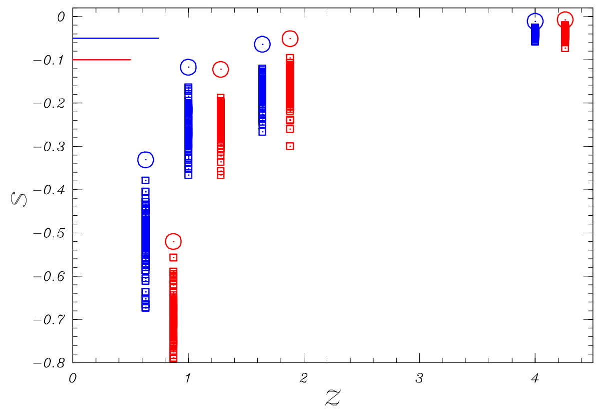

Figure 10: Entropy, s, plotted against downstream distance for circular (red) and slanted slot (blue) orifices. Each symbol represents an individual measurement. Also plotted (as open circles) is the entropy h at each station. Distances are measured from the center of the rows of orifices and the downstream extent of the orifices is indicated by the horizontal red and blue lines.

entropy are shown in Figure 10.

Plots such as Figure 9 allow us to locate the most typical snapshot in terms of mixedness and mixing rate: that is, the snapshot with coordinates (s_i, R_i) closest on the graph to the mean $(\langle s\rangle, \langle R\rangle)$. In fact, the typical snapshots shown in Figures 3 and 4 were selected in exactly this manner. These typical snapshots are clearly quite different from the mean concentration fields, $\bar{\rho}(\mathbf{x})$, in which only large scales survive, and are impossible to locate without an objective measure of mixing.

Summary

This paper has focused on the quantification of mixing and mixing rate. We have introduced new measures: the mixedness or "entropy", h, and the mixing rate, R. In many circumstances it is expected that the following relation holds:

$$\frac{dh}{dt} = 4\int(\kappa+\kappa_e)(\nabla\bar{\sigma}^{1/2})^2\,d\mathbf{x}\ . \tag{27}$$

The entropy was calculated for cross sectional measurements of a self-similar axisymmetric jet and was found to be constant along the jet, in agreement with scaling arguments.

The entropy and mixing rate were calculated for ensembles of concentrations collected at different locations in an experimental model of a gas combustor quench region. The wide variation in mixedness at any single station makes visual assessment of the degree of mixing difficult. The average entropy and mixing rate characterizes the flows and provides objective criteria to allow optimization of the orifice shape to promote rapid mixing.

Acknowledgment

We are grateful to Mr. David Liscinsky for providing us with the slot and hole data. Also we would like to express our thanks to Dr. J.D. Holdeman of NASA LERC for many useful discussions and for his support of this work. This work was supported by NASA Contract NAS3-25954, Task order #12 and by United Technologies Corporation.

References

[1] R.J Shaw. Engine technology for a 21st century high speed civil transport. In *AIAA 10th International Symposium on Air Breathing Engines*, September 1991.

[2] M.B. Long, B.T. Chu, and R.K. Chang. Instantaneous two-dimensional gas concentration measurements by light scattering. *AIAA Journal*, 19(9):1151–1157, 1981.

[3] M.C. Escoda and M.B. Long. Rayleigh scattering measurements of the gas concentration field in turbulent jets. *AIAA Journal*, 21:81–84, 1983.

[4] M.B. Long, D.C. Fourguette, M.C. Escoda, and C.B. Lane. Instantaneous Ramanography of a turbulent diffusion flame. *Optics Letters*, 8:244–246, 1983.

[5] M.J. Dyer and D.R. Crosley. Two-dimensional imaging of OH laser-induced fluorescence in a flame. *Optics Letters*, 7:382–384, 1982.

[6] A. Lozano, B. Yip, and R.K. Hanson. Acetone: a tracer for concentration measurements in gaseous flows by planar laser-induced fluorescence. *Experiments in fluids*, 13:369–376, 1992.

[7] B. Yip, A. Lozano, and R.K. Hanson. Gas phase molecular mixing measurements using the acetone-biacetyl system. In *AIAA–93-0221*, 1992.

[8] M. Winter, J.C. Hermanson, and G.M. Dobbs. Imaging of molecular mixing in a gas-phase turbulent jet by collisional energy-transfer fluorescence. In *AIAA–92-0381*, January 1992.

[9] W.J.A. Dahm and P.E. Dimotakis. Measurement of entrainment and mixing in turbulent jets. *AIAA Journal*, 25:1216–1223, 1987.

[10] M. Winter, T. Barber, R.M. Everson, and L. Sirovich. Eigenfunction analysis of turbulent mixing phenomena. *AIAA Journal*, 20(7):1681–1688, 1992.

[11] A. Vranos and D.S. Liscinsky. Planar imaging of jet mixing in crossflow. *AIAA Journal*, 26(11):1297–1298, 1988.

[12] D.S. Liscinsky, B. True, and J.D. Holderman. Mixing characteristics of directly opposed rows of jets injected normal to a crossflow in a rectangular duct. In *AIAA–94–0217*, January 1994.

[13] E.W. Schrodinger. *Statistical Thermodynamics*. Cambridge University Press, 1946.

[14] S. B. Pope. Probability distributions of scalars in turbulent shear flow. In J.S. Bradbury, F. Durst, F.W. Schmidt, and J.H. Whitelaw, editors, *Turbulent Shear Flows*, volume 2, pages 7–16, 1979.

[15] S. Chapman and T.G. Cowling. *The mathematical theory of non-uniform gases*. Cambridge University Press, 1939.